Atmos. Chem. Phys., 25, 8213–8228, 2025
https://doi.org/10.5194/acp-25-8213-2025

Atmospheric Chemistry and Physics
Open Access
EGU

Iron isotopes suggest significant aerosol dissolution over the Pacific Ocean

Capucine Camin[1], François Lacan[1], Catherine Pradoux[1], Marie Labatut[1], Anne Johansen[2], and James W. Murray[3]

[1]Université de Toulouse, LEGOS (CNES/CNRS/IRD/UT), Toulouse, France
[2]Department of Chemistry, Central Washington University, Ellensburg, Washington, USA
[3]School of Oceanography, University of Washington, Seattle, Washington, USA

Correspondence: Capucine Camin (capucine.camin@orange.fr) and François Lacan (francois.lacan@cnrs.fr)

Received: 2 December 2024 – Discussion started: 19 December 2024
Revised: 28 March 2025 – Accepted: 9 April 2025 – Published: 30 July 2025

Abstract. This study presents aerosol iron isotopic compositions (δ^{56}Fe) in the western and central equatorial and tropical Pacific Ocean. Aerosols supply iron (Fe), a critical element for marine primary production, to the open ocean. Particulate aerosols, > 1 µm, were sampled during the EUCFe (Equatorial Undercurrent Fe) cruise (RV *Kilo Moana*, PI: James W. Murray, 2006). One aerosol sample was isotopically lighter than the crust ($\delta^{56}\text{Fe} = -0.16 \pm 0.07$ ‰, 95 % confidence interval), possibly originating from combustion processes. The nine other aerosol samples were isotopically heavier than the crust, with a rather homogeneous signature of $+0.31 \pm 0.21$ ‰ (2 SD, $n = 9$). Given (i) this homogeneity compared to the diversity of their modeled geographic origin and (ii) the values of the Fe/Ti ratios used as a lithogenic tracer, we suggest that these heavy δ^{56}Fe signatures reflect isotopic fractionation of crustal aerosols caused by atmospheric processes. Using a fractionation factor of $\Delta_{\text{solution - particle}} = -1.8$ ‰, a partial dissolution of ≈ 13 % of the initial aerosol iron content, followed by the removal of this dissolved fraction, would explain the observed slightly heavy Fe isotope signatures. Such fractionation has been observed previously in laboratory experiments but never before in a natural environment. The removal of the dissolved fraction of the aerosols has not been previously documented either. This work illustrates the strong constraints provided by the use of iron isotopes for atmospheric process studies.

Key points.

- Iron isotope fractionation of particle aerosol during atmospheric transport
- Aerosol partial dissolution and subsequent removal of the dissolved fraction

1 Introduction

Iron (Fe) is an essential micronutrient for phytoplankton, playing a key role in primary production, nitrogen fixation, and community structures (Boyd and Ellwood, 2010; Morel et al., 2020). Availability and speciation of this micronutrient impact the global carbon cycle and climate. In some areas of the open ocean, low concentrations of Fe can limit primary production (Martin, 1992). Five predominant sources of bioavailable Fe to the global ocean are currently thought to be aerosol dissolution (Duce and Tindale, 1991; Jickells et al., 2005; Moore and Braucher, 2008), sediment dissolution and resuspension (Elrod et al., 2004; Radic et al., 2011; Labatut et al., 2014), fluvial inputs (Poulton and Raiswell, 2002), hydrothermal vents (Tagliabue et al., 2010; Resing et al., 2015), and local ice melting (Raiswell et al., 2008). Iron sources to the open ocean remain insufficiently understood.

Over the past 2 decades, it has become possible to measure iron isotopes in the environment. The isotopic composition is expressed by δ^{56}Fe in per mil (‰), which shows the deviation of the sample's ^{56}Fe/^{54}Fe ratio relative to the reference material IRMM-14 (Eq. 1):

$$\delta^{56}\text{Fe} = \frac{\left(^{56}\text{Fe}/^{54}\text{Fe}\right)_{\text{sample}}}{\left(^{56}\text{Fe}/^{54}\text{Fe}\right)_{\text{IRMM-14}}} - 1. \quad (1)$$

With this definition, the upper continental crust is characterized by a homogeneous signature of $\delta^{56}Fe = +0.07\,‰$ (Poitrasson, 2006). Iron isotope measurements have led to significant advances in our understanding of the cycle of this element (Radic et al., 2011; John et al., 2012; Conway and John, 2014; Ellwood et al., 2015; Abadie et al., 2017; Klar et al., 2018; Chen et al., 2020; Homoky et al., 2021). However, isotopic studies on aerosols in marine environments are still very rare.

Aerosols can be of natural or anthropogenic origins, each associated with variable ranges of Fe isotope signatures (Wang et al., 2022). Natural sources of aerosols are rocks, soils, loess, seawater, river water, volcanoes, plants, and biomass burning. For instance, lithogenic Fe isotopic compositions are in a narrow range between $-0.11\,‰$ and $+0.12\,‰$ (Beard et al., 2003). Anthropogenic aerosols are mainly derived from combustion processes such as coal combustion, metallurgy, waste incineration, and vehicle exhaust (Kommalapati and Valsaraj, 2009). These aerosols have been found to span a large range of $\delta^{56}Fe$ values, from $-3.91\,‰$ (Kurisu et al., 2016b) to $+0.80\,‰$ (Flament et al., 2008). Therefore, iron isotopes can be used to identify aerosol sources. Nevertheless, initial aerosol isotope signatures may be modified through isotope fractionations during atmospheric transport. Such fractionation can complicate the interpretation of isotopic signatures as source tracers. Laboratory experiments have documented Fe isotope fractionation due to aerosol partial dissolution (Mulholland et al., 2021; Maters et al., 2022). However, such fractionation has not been evidenced from in situ data. This is only one potential explanation among others to understand the iron isotope signature of aerosols during field study (Kurisu et al., 2021). Aerosol Fe isotopic data are scarce in oceanic environments, and no data have been reported in the equatorial Pacific, despite the important role of iron as a limiting micronutrient in the eastern equatorial Pacific.

This article presents iron isotope data from these aerosols collected in the equatorial and tropical Pacific. Combined with elemental concentration data and modeled back trajectories, these isotopic data provide new constraints on the processes involved in the aerosol iron cycle during atmospheric transport.

2 Sampling locations and methods

2.1 Aerosol sampling

Atmospheric particles were sampled during the EUCFe cruise (August–October 2006, R/V *Kilo Moana*, chief scientist James W. Murray). This cruise was carried out to study the iron cycle, including atmospheric deposition, in the equatorial and tropical Pacific (Slemons et al., 2009, 2010, 2012; Radic et al., 2011; Labatut et al., 2014). Samples were collected along the cruise track with a small volume collector equipped with 1 µm porosity, 47 mm diameter PTFE membranes, placed in a Millipore® polycarbonate filter holder. The membranes were pre-cleaned in ultrapure HNO_3 for 2 d and stored in clean plastic Petri dishes. The collector was located on the top deck and equipped with a control system to stop pumping when the wind came from a direction greater than 60° from the bow to prevent ship smoke collection. To protect the samples from rain, the filter support was angled downward and covered with a plastic protector. A flow meter provided information on the pumped airflow: 8 L min^{-1} for A281 and A284 samples and 28 L min^{-1} for the eight other samples. Each sample was collected over a duration of 3 d on average for sample size ranging between 9 and 93 m^3 (from coastal to open-ocean areas). The sampling locations are reported in Fig. 1. The sampling area is more than 8000 km wide.

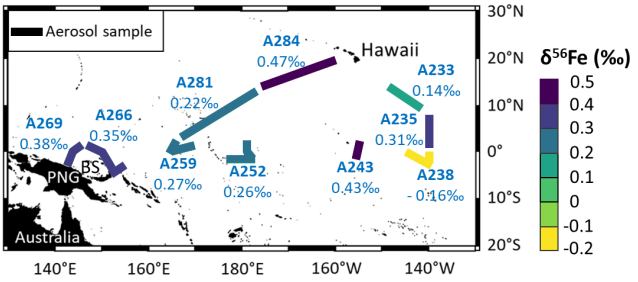

Figure 1. Location of aerosol samples. Aerosol sampling transects are shown by the thick lines. The Fe isotopic compositions are indicated by the color bar and under the sample names. PNG stands for Papua New Guinea. BS stands for Bismarck Sea.

Three samples previously published close to the Bismarck Sea and in the equatorial Pacific are reported to enrich the discussion: A269, A266, and A259 (Fig. 1 and Table 3) (Labatut et al., 2014).

2.2 Analytical procedure

The elemental concentrations and iron isotopic compositions were measured at the LEGOS laboratory (Observatoire Midi-Pyrénées, Toulouse, France) in the years 2009 to 2012. The analytical procedure was described by Labatut et al. (2014) and is summarized here. A trace metal clean laboratory, an ISO4 laminar flow hood, high-purity reagents, and acid-cleaned labware were used for all chemical procedures. The particles were totally digested using a mixture of 5 M HCl, 2.1 M HNO_3, and 0.6 M HF at 130 °C. To check that the procedure was quantitative, some filters were digested twice, and no particulate Fe was detected in the second leach. A ^{57}Fe–^{58}Fe double spike was added to the leachates. 2 % aliquots were taken for multi-elemental concentration determination on a ThermoScientific Element-XR HR-ICPMS. Na, Mg, Al, Ca, Ti, Fe, V, Rb, Sr, Ba, and Pb concentrations were quantified. Fe was purified from the remaining 98 % with an AG® 1-X4 anionic resin, and its isotopic composi-

tion and concentration were measured on a ThermoScientific Neptune MC-ICPMS.

Throughout this article, uncertainties are given at a 95 % confidence level. For the Fe concentration and isotope measurements on the Neptune MC-ICPMS, the total procedural recovery was 93 ± 25 %. The total procedural blank, including contamination from the sampling filter, was 3.0 ng, which was 3.8 % and 14.7 % of the average and smallest sample, respectively. Repeatability was not determined on aerosol samples (due to limited sample sizes) but was quantified during the same measurement sessions from duplicate analyses, including distinct chemical treatments, of four seawater suspended particle samples. It was 4 % and 0.04 ‰ for concentration and isotopic composition, respectively. This repeatability for δ^{56}Fe is better than the long-term external precision of 0.07 ‰ of our measurements, determined from repeated analysis of a secondary isotopic standard (an in-house "ETH-Hematite" standard). The uncertainties characterizing our Fe isotope data are therefore 0.07 ‰ or the internal measurement uncertainty (2 standard errors), when the latter is larger. The iron isotope protocol at LEGOS has been validated through intercalibration and intercomparison exercises (Boyle et al., 2012; Conway et al., 2016) and described in Lacan et al. (2008, 2010, 2021). The in-house "ETH-Hematite" standard displayed an isotopic composition of $+0.52 \pm 0.08$ ‰ (2 SD, $n = 81$), which was perfectly consistent with the recommended value of $+0.53 \pm 0.06$ ‰ (2 SD, $n = 6$) (Lacan et al., 2010). We also measured the sediment geostandard GBW 07315 with $\delta^{56}\text{Fe} = +0.04 \pm 0.046$ ‰. Unfortunately, it is not certified for Fe isotopes, and we could not find Fe isotope values reported in the literature. We still report it here as it could be useful in the future. The trueness of concentrations determined by HR-ICPMS analysis was verified using certified SLRS-5 river water material and GBW 07315 sediment material. The accuracy (trueness and repeatability) of our HR-ICPMS concentration determination was also validated through intercalibration exercises (Yeghicheyan et al., 2013, 2019). Blanks were quantified for Fe only. Based on the latter and assuming a crustal composition, they were estimated for the other elements. This assumption is supported by the lack of contamination discussed in Sect. 3.1 below. This leads to blank levels always lower than 15 % of each sample and all elements, except for Ca, for which it was 11.8 % on average and 35.7 % at maximum.

2.3 HYSPLIT model

To identify the origin of sampled aerosols, air mass back trajectories were calculated using the NOAA Hybrid Single-Particle Lagrangian Integrated Trajectory (HYSPLIT) model (Stein et al., 2015; Rolph et al., 2017). The meteorological data selected were from the Global Data Assimilation System (GDAS). Trajectories were computed at 50 m above ground level with a 7.5 d run time. Aerosol samplings were conducted between 22 August and 12 October 2006. In order to represent spatial and temporal variabilities and to present a synthetic overview, we divided the cruise track into four areas (Fig. 2).

For each area from which back trajectories are simulated, the starting points of back trajectories were chosen as a grid for representativity and clarity purposes. The grid points are not precisely sampling locations, but they are close to them. The starting times were chosen as the central dates between the sampling period of each area (Table 1).

3 Results

Elemental concentrations are presented in Table 2. Isotopic compositions of Fe in aerosols are reported in Table 3 and in Fig. 1. Fe concentration and isotope data are available in the SEANOE data repository (https://doi.org/10.17882/107774, Lacan et al., 2025) and will also be included in the GEOTRACES Data Product.

3.1 Elemental concentrations

Aerosol iron concentrations ranged from 0.38 ± 0.02 to 7.22 ± 0.28 ng m^{-3} (Table 2). Excluding aerosol sample A266 close to the Bismarck Sea (5.56 ± 0.22 ng m^{-3}), concentrations vary from low values (< 1 ng m^{-3}) between 140° E and 160° W along the Equator to large values (> 1.5 and < 8 ng m^{-3}) in the tropical North Pacific region and between 160 and 140° W along the Equator. There was no correlation between distance from land and concentration. A major volcanic eruption of Tavurvur (Papua New Guinea) occurred on 7 October 2006 (Wunderman, 2006). Samples A233 to A269 were collected prior to this event and are therefore unaffected. While it is theoretically possible that samples A281 and A284 could have been influenced by the eruption, they were collected over 1500 km away from the volcano. A simulation of the forward trajectory of air masses confirms that samples A281 and A284 were not affected by the eruption (Figs. A1 and A2). Additionally, their concentrations are consistent with those of samples collected before the eruption, confirming that they were not impacted.

Aerosol Fe concentrations in EUCFe samples are consistent with the literature in the central equatorial Pacific for particulate Fe: 2.01 ± 1.56 ng m^{-3} (2 SD, $n = 11$) (GEOTRACES GP15 cruise: between 20° N and 20° S and along the 152° W meridian) (Marsay et al., 2022) and 5.60 ± 5.65 ng m^{-3} (2 SD, $n = 8$) (P16 cruise of the CLIVAR/CO_2 Repeat Hydrography Program: between 9° N and 2° S and along the 151° W meridian) (Landing et al., 2013). The range of EUCFe values was also similar to concentrations in Alaskan coastal and pelagic regions in the subarctic North Pacific, in the North Pacific, and in the South Pacific (Buck et al., 2019; Kurisu et al., 2021, 2024; Marsay et al., 2022; Sakata et al., 2022). EUCFe data are lower than aerosol iron concentrations reported in the coastal northwest

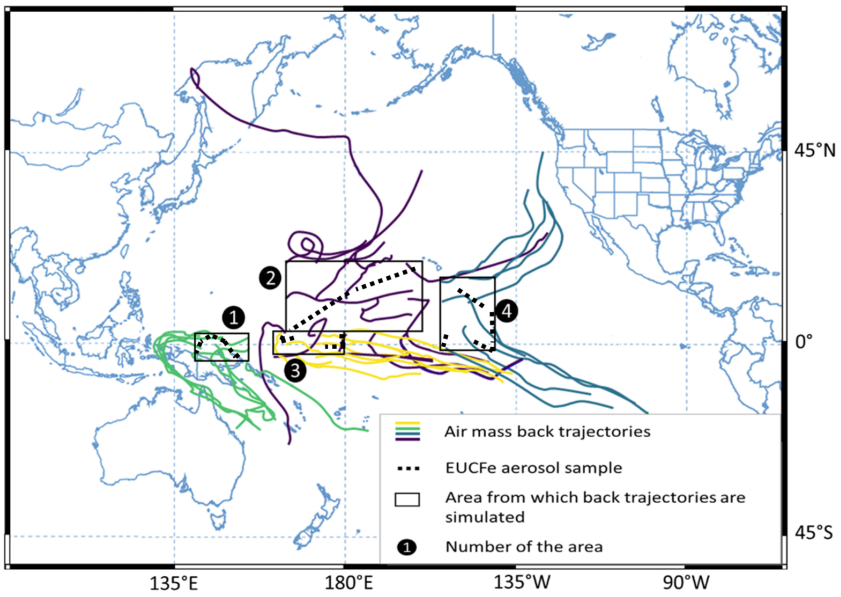

Figure 2. Air mass back trajectories (colors lines) calculated with the Hybrid Single-Particle Lagrangian Integrated Trajectory model (HYSPLIT, NOAA, and GDAS meteorological data). Trajectories were conducted at the height of 50 m (a.g.l.) with a 7.5 d run time. Each color is associated with an area from which back trajectories are simulated.

Table 1. Parameters selected for the HYSPLIT model simulations and the aerosol sample names within areas from which back trajectories are simulated.

Area number	Area – lower-left grid point	Area – upper-right grid point	Number of starting points within the area	Starting time	Aerosol samples within the area
1	142° E 4° S	154° E 2° N	9	25 Sep 2006, 16:00:00 UTC	A266, A269
2	164° E 3° N	160° W 21° N	15	11 Oct 2006, 16:00:00 UTC	A281, A284
3	164° E 3° S	180° 3° N	9	13 Sep 2006, 16:00:00 UTC	A252, A259
4	155° W 1° S	139° W 15° N	12	26 Aug 2006, 16:00:00 UTC	A233, A235, A238, A243

Pacific, closer to industrialized areas (Kurisu et al., 2021; Sakata et al., 2022).

The concentrations of the major elements of seawater (Na, Mg, Ca, Sr) depend on the height of sampling, wave height, and wind intensity (Bruch et al., 2021; Madawala et al., 2024). Therefore, comparing Na, Mg, Ca, and Sr concentrations in EUCFe samples with those measured in other Pacific samples is not meaningful. However, we can compare Al, Ti, V, and Pb elements with the literature. Their concentrations are in the same order of magnitude as those found previously in the atmosphere over the North Pacific (Kurisu et al., 2021, 2024). To the best of our knowledge, the EUCFe Rb and Ba concentrations are the first measurements over the Pacific Ocean. Their concentrations are similar to those of aerosols over the Atlantic Ocean (Landing and Shelley, 2014; Shelley et al., 2017). Given that V can be used as a tracer of the ship's exhaust (Duce and Hoffman, 1976), the lack of correlation between V concentrations and δ^{56}Fe (Fig. B2) ruled out the possibility of contamination from the ship's exhaust.

Overall, these comparisons are consistent with previous values for these elements and validate the analytical procedure, from sampling to final concentrations.

3.2 Iron isotopic compositions

EUCFe aerosols have Fe isotopic ratios ranging from −0.16 ‰ to +0.47 ‰ (Table 3, Figs. 1 and 3). Those sampled along the Equator and near the Bismarck Sea exhibit similar, slightly heavy signatures, ranging from +0.26 ‰ to +0.43 ‰. Those sampled in the tropical North Pacific present more variable signatures but are still positive from +0.14 ‰ to +0.47 ‰. One sample, the southeasternmost one (A238), differed significantly from the others in the equatorial Pacific with the lightest value, −0.16 ‰.

δ^{56}Fe aerosol values from the EUCFe cruise can be compared with three other cruises in the Pacific: KH-13-7 and KH-14-3 in the North Pacific (Kurisu et al., 2021) and GP02 in the subarctic North Pacific (Kurisu et al., 2024) (Fig. 3). In these previous studies, all δ^{56}Fe values below

Table 2. Aerosol elemental concentrations from the EUCFe cruise. Concentration uncertainty was 4 % (95 % confidence level). Some concentrations were found below quantification limits. In that case, they are reported after the "<" symbol. The mean concentrations do not take into account samples with a concentration below the quantification limits. Al concentration for the A252 sample (reported in brackets in the table) was suspected to be contaminated; it is not included in the mean calculation and in the discussion. UCC stands for upper continental crust. Note that the different detection limits for the same element are due to different sample volumes (m^3).

Samples	[Na] ng m^{-3}	[Mg] ng m^{-3}	[Ca] ng m^{-3}	[Sr] pg m^{-3}	[Ba] pg m^{-3}	[Al] ng m^{-3}	[Ti] ng m^{-3}	[V] pg m^{-3}	[Fe] ng m^{-3}	[Rb] pg m^{-3}	[Pb] pg m^{-3}
A233	135	17.5	13.4	170	37.4	2.42	0.30	5.91	1.71	< 22.3	11.1
A235	1085	128	64.9	1144	28.2	1.90	0.73	7.09	7.22	13.5	14.4
A238	3031	323	126	2169	272	20.3	0.59	13.4	3.81	58.7	17.2
A243	1021	114	49.0	730	372	26.1	0.50	< 49.9	2.28	45.5	< 63.2
A252	2432	223	85.4	1552	68.2	(188)	0.22	64.9	0.99	20.5	13.9
A259	809	77.6	36.1	520	< 40.9	0.76	0.20	4.77	0.38	< 28.8	10.7
A266	224	20	8.93	< 91.4	< 18.6	1.28	0.12	< 12.6	5.56	< 13.1	< 16.0
A269	121	12.5	4.94	84.6	17.9	2.19	0.11	< 16.6	0.54	< 17.2	19.9
A281	653	58.6	26.0	373	75.0	9.15	0.42	20.9	2.42	< 41.1	29.5
A284	1072	97.7	41.5	652	418	23.5	0.45	28.4	5.17	50.3	41.8
Mean concentrations of samples	1058	107	45.6	822	161	9.7	0.36	20.8	3.01	38	19.8
Mean UCC in g g^{-1} (Rudnick and Gao, 2014)	2.43×10^{-2}	1.50	2.57	3.20×10^{-4}	6.24×10^{-4}	8.15×10^{-2}	3.84×10^{-3}	9.70×10^{-5}	3.92×10^{-2}	8.40×10^{-5}	1.70×10^{-5}
Typical North Pacific concentrations in filtered seawater in ng kg^{-1} (Nozaki, 1997)	1.08×10^{10}	1.28×10^{9}	4.12×10^{8}	7.80×10^{6}	1.50×10^{4}	30.0	6.50	2.00×10^{3}	30.0	1.20×10^{5}	2.70

Table 3. Aerosol Fe isotopic compositions during the EUCFe cruise. U95 stands for measurement uncertainty at the 95 % confidence level.

Samples ID	Location	Sampling date	δ^{56}Fe (‰)	δ^{56}Fe U95 (‰)
A233	from 12.39° N, 149.54° W to 06.01° N, 143.42° W	21–23 Aug 2006	+0.14	0.07
A235	from 06.01° N, 143.42° W to 01.07° N, 140.00° W	23–25 Aug 2006	+0.31	0.07
A238	from 00.0° N, 140.0° W to 00.52° S, 144.15° W	26–28 Aug 2006	−0.16	0.07
A243	from 01.02° N, 154.60° W to 01.31° S, 155.00° W	31 Aug–1 Sep 2006	+0.43	0.07
A252	from 02.02° N, 180.00° E to 01.22° S, 178.16° E	9–11 Sep 2006	+0.26	0.07
A259*	from 01.48° N, 167.31° E to 01.06° N, 164.59° E	16–17 Sep 2006	+0.27	0.15
A266*	from 02.32° S, 153.56° E to 01.18° N, 146.34° E	23–25 Sep 2006	+0.35	0.07
A269*	from 01.18° N, 146.33° E to 03.21° S, 143.52° E	26–28 Sep 2006	+0.38	0.08
A281	from 03.39° N, 167.55° E to 13.02° N, 175.06° W	8–11 Oct 2006	+0.22	0.09
A284	from 14.20° N, 173.5° W to 20.20° N, 160.50° W	11–14 Oct 2006	+0.47	0.08

* Identifies data previously published by Labatut et al. (2014).

0 ‰ were measured in samples taken less than 1500 km from the Japanese and Alaskan coasts (Fig. 3). In the open ocean, they also reported positive δ^{56}Fe values as for EUCFe samples (apart from sample A238). South of the Tropic of Cancer, Kurisu et al. (2021) reported bulk aerosol heavy δ^{56}Fe values, between +0.04 ‰ and +0.42 ‰, with a mean value of $+0.27 \pm 0.26$ ‰ (2 SD, $n = 7$). In the subarctic North Pacific, the pelagic and Alaskan areas have δ^{56}Fe values between −0.07 ‰ and +0.45 ‰ (Kurisu et al., 2024). Overall, EUCFe δ^{56}Fe values are in excellent agreement with these previous works.

4 Discussion

All our aerosol samples, except the southeastern one (A238), are enriched in heavy isotopes relative to the crustal value. On average those are characterized by $\delta^{56}\text{Fe} \approx +0.31 \pm 0.21$ ‰ (2 SD, $n = 9$) (average value except A238, Table 3 and Fig. 1). The value for sample A238 was $\delta^{56}\text{Fe} = -0.16$ ‰.

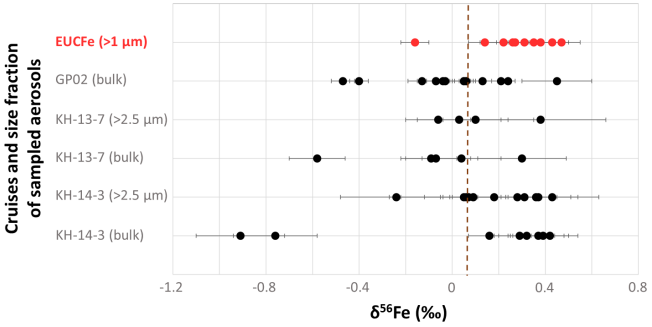

Figure 3. δ^{56}Fe (‰) of sampled aerosols during EUCFe in the equatorial and tropical Pacific, GP02 in the subarctic North Pacific (Kurisu et al., 2024), and KH-13-7 and KH-14-3 cruises in the North Pacific (Kurisu et al., 2021). Error bars represent 2 SD (‰) for EUCFe and GP02 cruises and 2 SE (‰) for KH-13-7 and KH-14-3 cruises. 2 SE only reflects the dispersions of the MC-ICPMS treatment. The vertical brown line indicates the upper crust value, +0.07 ‰ (Poitrasson, 2006).

4.1 Sources signatures

First, we will discuss the possibility that aerosol signatures correspond to unmodified source signatures. We will explore three hypotheses: contributions (i) from sea spray, (ii) from crustal sources, and (iii) from anthropogenic sources.

A first hypothesis is a contribution from seawater, i.e., sea spray. Based on the assumptions that all Na in EUCFe samples comes from seawater and that the chemical composition of sea spray is that of North Pacific seawater (Nozaki, 1997), the contribution of sea spray to our samples can be estimated with the following equation (Eq. 2):

$$\left[\mathrm{EI}_{\text{sea spray}}\right] = \left[\mathrm{Na}_{\text{sample}}\right] \frac{\left[\mathrm{EI}_{\text{SW-ref}}\right]}{\left[\mathrm{Na}_{\text{SW-ref}}\right]}, \quad (2)$$

where EI is the element of interest (Fe for instance) and SW-ref is the seawater used as a reference (Nozaki, 1997) for Na and EI (Table 2).

This leads to insignificant contributions from seawater to the Fe content of all our samples (lower than 10^{-5} % of the total Fe content) (Table C1). On the other hand, the estimated sea spray contribution for Mg, Ca, and Sr was > 89 % for all samples.

A second hypothesis is a source from the erosion products of crustal rocks. The crustal signature, $\delta^{56}\mathrm{Fe} = +0.07$ ‰, has been characterized in granites (Poitrasson, 2006), but other materials, such as volcanic rocks, exhibit similar isotopic composition. Desert dust, e.g., of Saharan origin (Beard et al., 2003; Waeles et al., 2007; Mead et al., 2013; Conway et al., 2019), and basalts (Poitrasson, 2006; Craddock et al., 2013; Teng et al., 2013) display the same signature. Accordingly, runoff water collected from the flanks of volcano Rabaul in the Bismarck area has been characterized by $\delta^{56}\mathrm{Fe} = +0.07 \pm 0.03$ ‰ (2 SD, $n = 2$) (Labatut et al., 2014). Therefore, EUCFe aerosol sample isotopic signatures, whether those in the group of nine samples slightly enriched in heavy isotopes or that of the A238 sample slightly enriched in light isotopes, do not directly reflect a crustal source.

A third hypothesis is an anthropogenic origin. Human activities emit aerosols within a wide range of δ^{56}Fe. On the one hand, vehicle exhaust, steel manufacturing, and solid waste incineration have been characterized by negative δ^{56}Fe signatures (Kurisu et al., 2016a). On the other hand, coal fly ash, metallic brake dust, and steel manufacturing have been characterized by positive δ^{56}Fe signatures (Flament et al., 2008; Majestic et al., 2009; Mead et al., 2013; Li et al., 2022). Biomass burning can be characterized by both negative δ^{56}Fe signatures (Mead et al., 2013) and positive δ^{56}Fe signatures, with the latter due to the presence of suspended soil particles (Kurisu and Takahashi, 2019).

Sample A238 ($\delta^{56}\mathrm{Fe} = -0.16$ ‰) is located in the southern part of the Pacific around 140° W (Figs. 1 and 3, Table 3). The air mass back trajectories (Fig. 2) suggest that aerosols collected in this area originated from the South Pacific or the South American coast. As stated above, several anthropogenic sources, biomass burning, vehicle exhaust, steel manufacturing, and solid waste incineration have been characterized by negative signatures (Mead et al., 2013; Kurisu et al., 2016a; Kurisu and Takahashi, 2019). Combustion processes from South America are therefore a potential explanation for the A238 sample.

The remaining of the discussion will focus on the group of nine samples, characterized by slightly heavy Fe isotopic composition ($\delta^{56}\mathrm{Fe} = +0.31 \pm 0.21$ ‰, 2 SD, $n = 9$; Figs. 1 and 3, Table 3). From a purely isotopic signature point of view, anthropogenic sources, e.g., coal combustion and steel manufacturing, possibly mixed with crustal sources, could explain these slightly heavy signatures (Wei et al., 2024). Nevertheless, there are several arguments contradicting this hypothesis: demography, modeled atmospheric back trajectories, aerosol size (> 1 µm), and elemental ratios such as Fe/Ti. While discussing similar slightly heavy aerosol isotopic signatures in the Bismarck Sea, a possible anthropogenic pollution contribution was excluded (Labatut et al., 2014) given the very low demography of the surrounding lands such as Papua New Guinea (Brunskill, 2004). Back trajectories presented in Fig. 2 reveal that the sampled air masses had a wide variety of geographic origins. The fact that aerosols have variable sources but similar isotope signatures does not support the hypothesis of an anthropogenic source such as coal fly ash, metallic brake dust, and steel manufacturing, which are not expected to be widely and homogeneously distributed around our study area. The separation between fine and coarse aerosol particles is 2 to 2.5 µm (Whitby, 1978; Seinfeld and Pandis, 2006). Nevertheless, fine particles do not ordinarily grow larger than 1 µm (Whitby, 1978). The EUCFe samples are mainly coarse aerosols, a size fraction associated with crustal sources (Mead et al., 2013). The Fe fractional solubility of

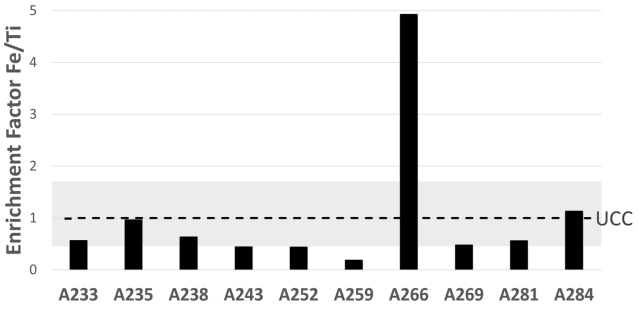

Figure 4. Enrichment factors for Fe relative to Ti in the EUCFe samples, in the UCC reference (dashed line) (Rudnick and Gao, 2014), and in eight UCC types of rocks (gray band) (Hu and Gao, 2008).

aerosols was not measured. While this would have been interesting, it is not critical, as this information alone is not necessarily indicative of aerosol sources (Baker and Jickells, 2006; Conway et al., 2015).

The enrichment factor (EF) in an element of interest relative to the crust (Zoller et al., 1974) can be defined as (Eq. 3):

$$\text{enrichment factor (EF)} = \frac{\left(\frac{\text{element of interest}}{\text{lithogenic tracer}}\right)_{\text{sample}}}{\left(\frac{\text{element of interest}}{\text{lithogenic tracer}}\right)_{\text{UCC}}}. \quad (3)$$

UCC stands for upper continental crust (Rudnick and Gao, 2014) (Table 2). Ti and Al are often used as lithogenic tracers (Dammshäuser, 2012). Because one sample (A252) is suspected to be contaminated in Al (Table 2), we chose Ti to calculate the EF relative to the crust in the following. Average UCC concentrations are often used as a reference (Rudnick and Gao, 2014). Nevertheless, the UCC exhibits variability in its elemental concentrations, which accounts for the range of Fe/Ti ratios depicted as a gray band in Fig. 4 (Hu and Gao, 2008). This range reflects eight types of rocks ($n = 40$), offering a non-exhaustive but more representative overview of the UCC.

Eight of the EUCFe samples fall within the UCC range (Fig. 4). However, two samples exhibit slightly lower (A259) and higher (A266) ratios. Their concentrations of anthropogenic tracers (Pb, V) do not suggest stronger anthropogenic contributions than in the other samples. The Fe/Ti ratios, which fall slightly outside the classical range (Hu and Gao, 2008) in samples A259 and A266, can nonetheless be explained by ultramafic rocks (e.g., pyroxenites), volcanic rocks (e.g., basalts and andesites), metamorphic rocks (e.g., gneiss), or plutonic rocks (e.g., diorite) (Turekian and Wedepohl, 1961; Canil and Lacourse, 2011). These rock types are present around the study area, notably the widespread volcanic rocks (Nusantara, 2000; Neall and Trewick, 2008; Ramos, 2009; Canil and Lacourse, 2011). Thus, despite the variable Fe/Ti ratios in our ten samples, they are all consistent with a crustal origin. Although it is common practice to use Pb or V enrichment factors relative to lithogenic tracers (such as Al or Ti) to trace anthropogenic sources, we chose not to do so because anthropogenic enrichments in Pb or V do not necessarily imply a significant anthropogenic enrichment in Fe (Table D1). Their use may therefore be misleading when studying the Fe cycle specifically.

Note that while the Fe/Ti A238 ratio is consistent with a crustal origin, it is also consistent with, for example, biomass burning (Zhai et al., 2021).

Based on the assumptions that all Ti in EUCFe samples comes from the UCC and that the chemical composition of crustal aerosol is that of UCC (Rudnick and Gao, 2014) (Table 2), the lithogenic contribution to our samples can be estimated (adjusting Eq. 2 to the case of a lithogenic source). For Fe, this leads to high lithogenic contributions (123 % on average). The fact that this calculation leads to contributions larger than 100 % likely reflects source ratios which differ from that chosen above (UCC) and/or Fe removal during transport.

These arguments suggest that the slightly heavy iron isotopic compositions are unlikely to be explained by anthropogenic sources but mainly by crustal ones. We will discuss below if our observations ($\delta^{56}\text{Fe}_{\text{average}} = +0.31\,‰$) can be explained by aerosols of crustal origin ($+0.07\,‰$) whose isotopic signature has been modified by isotopic fractionation during atmospheric transport.

4.2 Isotopic fractionation during atmospheric processes

A major process influencing aerosol chemistry, during atmospheric transport, is partial dissolution during condensation/evaporation cycles in clouds (Lelieveld and Crutzen, 1991; Desboeufs, 2001). Atmospheric aerosol Fe dissolution is mainly due to dissolution by low-pH cloud water and effects of solar irradiation. Different dissolution mechanisms exist, including proton-promoted (Chapman et al., 2009; Kiczka et al., 2010), ligand-promoted (Chapman et al., 2009; Kiczka et al., 2010; Mulholland et al., 2021; Maters et al., 2022), and reductive ligand-promoted dissolution (Mulholland et al., 2021; Maters et al., 2022). These processes fractionate iron isotopes (Mulholland et al., 2021; Maters et al., 2022). In most studies, light iron isotopes are preferentially dissolved, and the isotopic composition of the remaining particulate iron becomes gradually heavier (Maters et al., 2022) (Fig. 5). In the following, the notation $\Delta^{56}\text{Fe}_{\text{solution}-\text{particle}}$ is used to denote the isotopic fractionation characterizing a given dissolution process, also named the initial fractionation step or the enrichment factor (also note ε, Wiederhold et al., 2006; Maters et al., 2022).

The magnitude of the isotope fractionations, $\Delta^{56}\text{Fe}_{\text{solution}-\text{particle}}$, were found between $-0.3\,‰$ and $-2.0\,‰$ for biotite and chlorite mineral dissolution (Kiczka et al., 2010) and at $-1.95\,‰$ for granite dissolution by hydrochloric acid (Chapman et al., 2009). An experiment dissolving anthropogenic aerosols with a synthetic cloud

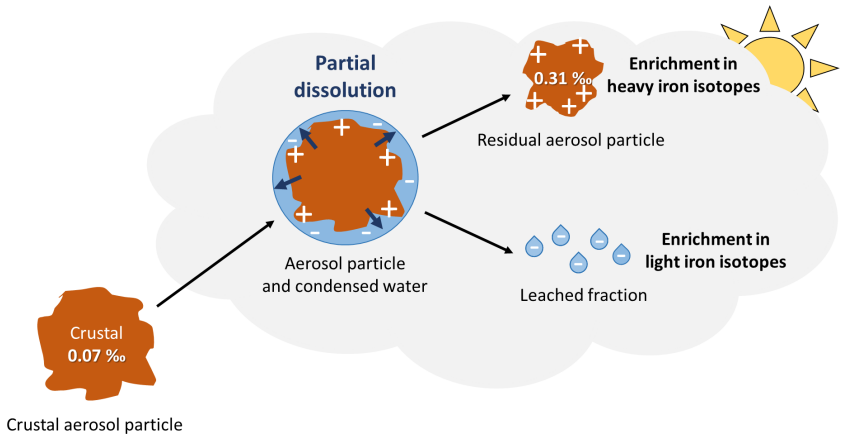

Figure 5. Path of an aerosol during atmospheric transport undergoing partial dissolution. Partial dissolution and subsequent separation of the leached fraction lead the residual particle to an enrichment in heavy and light iron isotopes in the particles and leached fraction, respectively.

water solution showed a preferential release of light isotopes with $\Delta^{56}Fe_{solution-particle} = -1‰$ (Mulholland et al., 2021). Another experiment of mineral dust and industrial ash dissolution in simulated cloud water also showed an enrichment in light Fe isotopes in solution, with an isotope fractionation $\Delta^{56}Fe_{solution-particle}$ of $-1.8‰$ for ash and dust (Maters et al., 2022). Thus, mineral dissolution appears to favor light isotopes, thereby enriching the remaining solid fraction in heavy isotopes. Therefore, we will assess whether partial dissolution during clouds transport can produce aerosols with a heavier iron isotopic composition. Some authors have suggested that the observed isotopic compositions may be partly due to isotopic fractionation during transport (Kurisu et al., 2021, 2024; Wang et al., 2022).

Considering that the leachate is isolated from the solid fraction of the aerosol, the system can be modeled as a Rayleigh distillation. The isotope composition of the solid fraction of the aerosol is calculated according to Eqs. (4) and (5):

$$(\delta^{56}Fe_{particle})_f \approx (\delta^{56}Fe_{particle})_{f=1} + \Delta^{56}Fe_{solution-particle}\ln(f), \quad (4)$$

where the particle is the solid fraction of the aerosol, the solution is the leached solution, and f is the remaining fraction of $Fe_{particle}$ (when $f = 1$ all Fe is in the particle; no Fe has been leached).

For the particle value, we assume an initial crustal signature for EUCFe aerosols, $(\delta^{56}Fe_{particle})_{f=1} = +0.07‰$ (Poitrasson, 2006). For the isotopic fractionation, $\Delta^{56}Fe_{solution-particle}$, although the experiments described above document values ranging between $-2.0‰$ and $-0.3‰$, we choose $-1.8‰$ (Maters et al., 2022). This value was measured during a laboratory experiment on dust with simulated cloud water, i.e., a similar situation to the EUCFe field study (Maters et al., 2022). Equation (5) (derived from Eq. 4) allows us to estimate the fractions of the particles that have to be dissolved $(1 - f)$ in order to reach the slightly heavy isotope composition measured.

$$1 - f = 1 - e^{\frac{(\delta^{56}Fe_{particle})_{f=1} - (\delta^{56}Fe_{particle})_f}{\Delta^{56}Fe_{solution-particle}}} \quad (5)$$

Based on these calculations, we estimate Fe dissolution percentages varying from 4 % to 20 % with an average value of 13 % (Table 4). This is the first estimate of this kind to our knowledge. A comparison can be made with Fe fractional solubility of aerosols measured during seawater or ultrapure deionized water leaching experiments (Sholkovitz et al., 2012; Buck et al., 2013; Shelley et al., 2018; Kurisu et al., 2021, 2024; Desboeufs et al., 2024), keeping in mind that clouds are slightly acidic with a pH around 5 in the equatorial Pacific (Shah et al., 2020). Locally, Fe fractional solubility can reach 23 % in the northwestern Pacific (Kurisu et al., 2021) and 29 % in the Pacific Ocean (3 cruises) (Buck et al., 2013) during leaching experiments with ultrapure deionized water. Mean Fe fractional solubility has been reported as the highest in the world in the equatorial Pacific, with mean values ranging from 12 % to 20 % (Hamilton et al., 2019). Fe fractional solubility depends on numerous factors such as aerosol size and origin, as well as atmospheric processes (pH, solar irradiation, composition of the solution). Crustal aerosols collected during dust events in coastal Namibia (aerosols $< 10\,\mu m$) can reach high Fe fractional solubilities of 20 % (Desboeufs et al., 2024). Therefore, a 13 % dissolution is a realistic value for crustal aerosols.

An isotopic fractionation by partial dissolution of crustal origin aerosols could therefore explain the slightly heavy signatures observed (Fig. 5). This would require that the leached fraction, enriched in light isotopes, is separated from the solid fraction. In the absence of separation, the effect of isotope fractionation would not have been measured in our samples. This process has not yet been demonstrated, but the hypothesis has already been proposed in two publications

Table 4. Percentage of Fe dissolution ($1-f$) necessary to explain the observed EUCFe δ^{56}Fe through atmospheric isotopic fractionation from initial isotope signature of the upper crust (+0.07 ‰). Calculations are performed for all our samples except A238.

Samples	$(\delta^{56}Fe_{particle})_f$ (‰)	$1-f$ (%)
A233	+0.14	4
A235	+0.31	12
A243	+0.43	18
A252	+0.26	10
A259	+0.27	11
A266	+0.35	14
A269	+0.38	16
A281	+0.22	8
A284	+0.47	20
Average of all the above samples	+0.31	13

(Kurisu et al., 2021, 2024). The processes that could lead to such separation are difficult to identify. They are, however, necessary to explain our observations, provided that aerosol original signatures were crustal. Shattering or ice breaking are two ways to separate the leached fraction and the residual particle of the aerosols. Their occurrence is understudied, especially regarding shattering process. The enrichment of light isotopes in the leached fraction was not observed in this study. This is likely due to the presence of this fraction in aerosols smaller than 1 µm produced by ice-breaking or shattering processes (or its removal by wet deposition), which were not sampled during the EUCFe cruise. The Fe isotopic composition of fine aerosols, often negative, is mostly attributed to anthropogenic sources (Conway et al., 2019; Kurisu et al., 2021). However, this study proposes a new possible cause for the light Fe isotopic composition of aerosols smaller than 1 µm: the residual leached fractions of crustal aerosols. In the above model, isotopic fractionation applies to the whole particle (its entire mass), whereas in reality it is a surface process that only affects a peripheral layer. Taking into account surface processes would lead to smaller isotopic effects (Wiederhold et al., 2006). Our approximation led to an overestimation of the effect of isotope fractionation and therefore an underestimation of the leached fraction.

5 Conclusion

Fe isotope compositions (δ^{56}Fe) and elemental concentrations (Na, Mg, Al, Ca, Ti, Fe, V, Rb, Sr, Ba, and Pb) were analyzed in atmospheric particles collected during the EUCFe expedition in the equatorial and tropical Pacific, between Hawaii, the Equator, and Papua New Guinea. In all aerosol samples, with one exception, Fe is enriched in heavy isotopes relative to the crustal value, with an average δ^{56}Fe value of $+0.31 \pm 0.21$ ‰ (2 SD, $n = 9$). The simulation of air mass back trajectories, the size of particles, their chemical composition compared to potential sources (enrichment factors), and the geographic environment were used to help explain the enrichment in heavy Fe isotopes. An anthropogenic origin is unlikely due to (i) the homogeneity of aerosol delta values despite a wide variety of modeled geographic origin and (ii) the aerosol chemical composition. We conclude that these observations are best explained by crustal aerosols, with an initial isotope signature of δ^{56}Fe = +0.07 ‰, modified during atmospheric transport by partial dissolution followed by the removal of the leached fraction. Although such removal had not been previously reported, such Fe isotope fractionation has been documented in controlled experiments (Mulholland et al., 2021; Maters et al., 2022) and has already been suggested as one of several explanations for in situ data (Kurisu et al., 2021, 2024). The extent of Fe isotope fractionation during atmospheric transport requires the dissolution and removal of 4 % to 20% – 13 % on average – of the initial aerosol Fe contents.

One aerosol sample stands out by a slightly light isotopic composition of −0.16 ‰, possibly emitted from combustion processes in South America.

This highlights the challenging use of iron isotopes to trace the origin of the aerosols. It also highlights the unique and strong constraints brought by these isotopes on the Fe cycle in atmospheric aerosols. Further studies are needed to confirm the main conclusion of this study, namely the existence of processes leading to the removal of a significant fraction of the iron content of atmospheric aerosols during atmospheric transport.

Appendix A

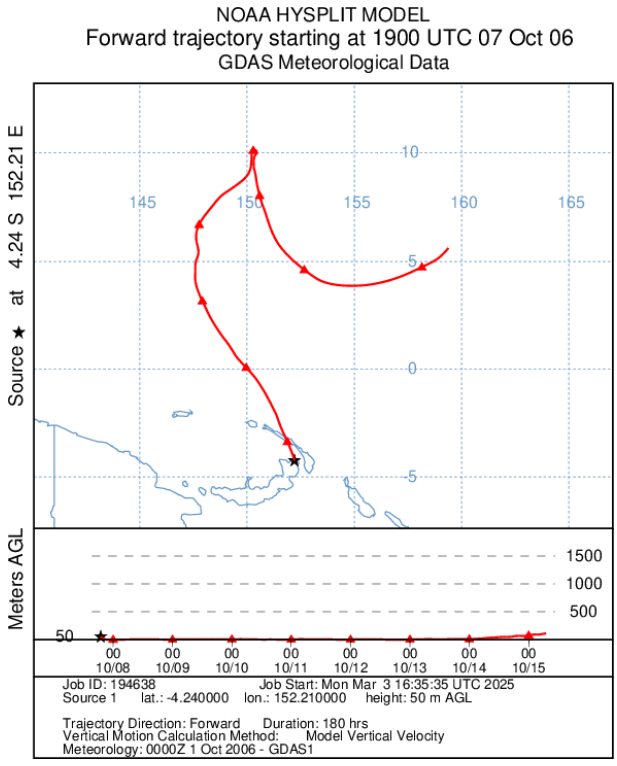

Figure A1. Air mass forward trajectory (red line) calculated with the Hybrid Single-Particle Lagrangian Integrated Trajectory model (HYSPLIT, NOAA, and GDAS meteorological data). The trajectory was conducted at the height of 50 m (a.g.l.) with a 7.5 d run time. The starting point of the trajectory is the Tavurvur volcano at 09:00 PGT (UTC + 10) on 7 October 2006, when the eruption began (Wunderman, 2006).

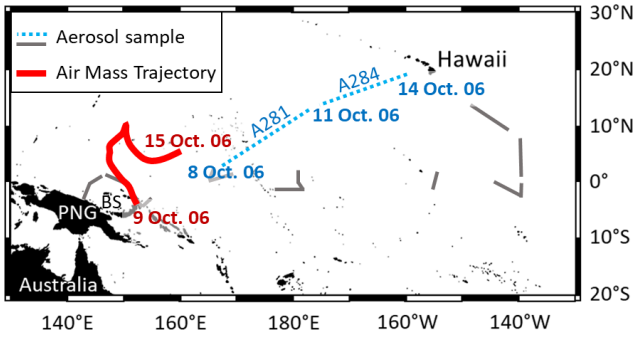

Figure A2. Reproduction of the forward trajectory (Fig. A1) on the aerosol sampling map. The starting point of the forward trajectory is the Tavurvur volcano at 09:00 PGT (UTC + 10) on 7 October 2006, when the eruption began (Wunderman, 2006). The ending point of the trajectory is on 15 October 2006. Aerosol samples on dashed lines (A281 and A284) are the only samples collected after the eruption, between 8 and 14 October 2006. PNG stands for Papua New Guinea. BS stands for Bismarck Sea.

Appendix B

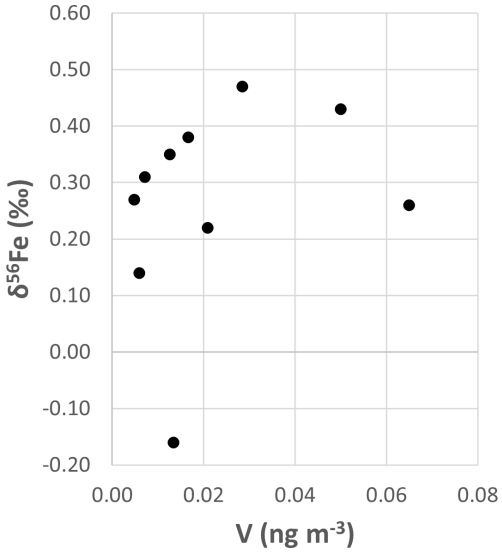

Figure B1. Fe isotopic composition (δ^{56}Fe) and Vanadium (V) concentrations of EUCFe aerosol samples. Measurement uncertainties can be found in Tables 2 and 3.

Appendix C

Table C1. Na concentrations (ng m^{-3}) and contribution of sea spray (%) to the Fe content of EUCFe samples.

Samples ID	[Na] (ng m^{-3})	Fe from sea spray (%)
A233	17.5	2.19×10^{-7}
A235	128	4.18×10^{-7}
A238	323	2.21×10^{-6}
A243	114	1.25×10^{-6}
A252	223	6.84×10^{-6}
A259	77.6	5.92×10^{-6}
A266	20	1.12×10^{-7}
A269	12.5	6.23×10^{-7}
A281	58.6	7.51×10^{-7}
A284	97.7	5.77×10^{-7}

Appendix D: Calculation of the relative contribution of two sources from elemental mass ratios (e.g., Pb/Fe)

In the hypothesis of a two-end-member mixing, when the mass ratios of two elements are known in the two sources and in the mixture, then the contribution of each source to the mixture can be calculated for the two elements.

Below, the two sources are named "source 1" and "source 2" and the mixture is named "sample".

QPb and QFe are quantities (ng) and [Pb] and [Fe] are concentrations (ng m^{-3}). $\frac{QPb}{QFe}_{sample}$, $\frac{QPb}{QFe}_{source\ 1}$, and $\frac{QPb}{QFe}_{source\ 2}$ are known.

Two-end-member mixing implies

$$\frac{QPb}{QFe}_{sample} = \frac{QPb_{source\ 1} + QPb_{source\ 2}}{QFe_{source\ 1} + QFe_{source\ 2}}.$$

This is equivalent to

$$\frac{QPb}{QFe}_{sample} = \frac{QFe_{source\ 1} \times \frac{QPb_{source\ 1}}{QFe_{source\ 1}} + QFe_{source\ 2} \times \frac{QPb_{source\ 2}}{QFe_{source\ 2}}}{QFe_{source\ 1} + QFe_{source\ 2}},$$

with $x = \frac{QFe_{source\ 1}}{QFe_{source\ 2}}$ the mass ratio in the sample.

$$\frac{QPb}{QFe}_{sample} = \frac{QFe_{source\ 1} \times \frac{QPb_{source\ 1}}{QFe_{source\ 1}} + \frac{QFe_{source\ 1}}{x} \times \frac{QPb_{source\ 2}}{QFe_{source\ 2}}}{QFe_{source\ 1} + \frac{QFe_{source\ 1}}{x}}$$

This is equivalent to

$$\frac{QPb}{QFe}_{sample} = \frac{\frac{QPb_{source\ 1}}{QFe_{source\ 1}} + \frac{1}{x} \times \frac{QPb_{source\ 2}}{QFe_{source\ 2}}}{1 + \frac{1}{x}}.$$

Therefore,

$$x = \frac{\left(\frac{QPb}{QFe}\right) sample - \left(\frac{QPb}{QFe}\right) source\,2}{\left(\frac{QPb}{QFe}\right) source\,1 - \left(\frac{QPb}{QFe}\right) sample}.$$

With this formula, we can calculate the anthropogenic and crustal contributions for both Fe and Pb in our samples given that the ratios are known in the two sources.

Below we illustrate our point with an example. For the anthropogenic source, we used data from Hao et al. (2007). This study was chosen for three main reasons: (1) the study area is relevant to our research – Qingdao, China (550 km from Beijing), a city with 2.3 million inhabitants; (2) the authors explicitly identify Pb as representing pollution and Fe as indicative of soil sources; and (3) the study provides elemental concentrations for each sample, allowing us to calculate Pb/Fe mass ratios, unlike most studies that only report mean concentrations. For the crustal source, we used the average of ratios found in eight different types of rocks from the UCC (Hu and Gao, 2008). The element ratios of these sources are 0.00095 g g^{-1} for the crustal source and 0.182 g g^{-1} for the anthropogenic source (roughly 200 times higher than the UCC). We applied these calculations to EUCFe samples, and results are shown in Table D1.

Table D1. Contribution of the anthropogenic source to the Fe and Pb content of EUCFe samples (%w w^{-1}). The Pb/Fe ratios are 0.00095 g g^{-1} for the UCC source (Hu and Gao, 2008) and 0.182 g g^{-1} for the anthropogenic source (Hao et al., 2007). ND: not determined.

Contribution (%w w^{-1}) of the anthropogenic source to the content of	EUCFe samples										
	A233	A235	A238	A243	A252	A259	A266	A269	A281	A284	Average
Fe	3 %	1 %	2 %	ND	7 %	15 %	ND	20 %	6 %	4 %	7 %
Pb	86 %	53 %	79 %	ND	94 %	97 %	ND	98 %	93 %	89 %	86 %

Code availability. Information on the software code used for the HYSPLIT back-trajectory model is available in the following articles: Stein et al. (2015) and Rolph et al. (2017).

Data availability. All the data used in this article are reported in Tables 2 and 3. Fe concentration and isotope data are available in the SEANOE data repository (https://doi.org/10.17882/107774, Lacan et al., 2025) and will also be included in the GEOTRACES Data Product.

Author contributions. JWM was the principal investigator of the EUCFe cruise. FL conceived the iron isotope work. AJ supervised the aerosol collection. ML, CP, and FL analyzed the samples. CC and FL wrote the article. All co-authors reviewed the manuscript.

Competing interests. The contact author has declared that none of the authors has any competing interests.

Disclaimer. Publisher's note: Copernicus Publications remains neutral with regard to jurisdictional claims made in the text, published maps, institutional affiliations, or any other geographical representation in this paper. While Copernicus Publications makes every effort to include appropriate place names, the final responsibility lies with the authors.

Acknowledgements. Amandine Radic is very much thanked for having carried out a part of the isotope work. Lindsey Shank is deeply thanked for having carried out the aerosol sampling on board. Jérôme Chmeleff, Frédéric Candaudap, and Aurélie Marquet are thanked for their support with the ICPMS at the *Observatoire Midi-Pyrénées*. The captain and the crew of the R/V *Kilo Moana* and especially the marine technicians Gabe Foreman and Daniel Fitzgerald are greatly acknowledged. The two anonymous reviewers are thanked for their comments, which significantly improved the manuscript.

Financial support. This study was funded by French and USA public funds. This study was also supported by the CNRS (French National Center for Scientific Research) and the University of Toulouse (France). The EUCFe expedition on the R/V *Kilo Moana* was supported by NSF OCE 0425721 (USA). The Fe isotope project was funded by the CNRS-INSU ISOFERIX project.

Review statement. This paper was edited by Markus Ammann and reviewed by two anonymous referees.

References

Abadie, C., Lacan, F., Radic, A., Pradoux, C., and Poitrasson, F.: Iron isotopes reveal distinct dissolved iron sources and pathways in the intermediate versus deep Southern Ocean, P. Natl. Acad. Sci. USA, 114, 858–863, https://doi.org/10.1073/pnas.1603107114, 2017.

Baker, A. R. and Jickells, T. D.: Mineral particle size as a control on aerosol iron solubility, Geophys. Res. Lett., 33, L17608, https://doi.org/10.1029/2006GL026557, 2006.

Beard, B. L., Johnson, C. M., Skulan, J. L., Nealson, K. H., Cox, L., and Sun, H.: Application of Fe isotopes to tracing the geochemical and biological cycling of Fe, Chem. Geol., 195, 87–117, https://doi.org/10.1016/S0009-2541(02)00390-X, 2003.

Boyd, P. W. and Ellwood, M. J.: The biogeochemical cycle of iron in the ocean, Nat. Geosci., 3, 675–682, https://doi.org/10.1038/ngeo964, 2010.

Boyle, E. A., John, S., Abouchami, W., Adkins, J. F., Echegoyen-Sanz, Y., Ellwood, M., Flegal, A. R., Fornace, K., Gallon, C., Galer, S., Gault-Ringold, M., Lacan, F., Radic, A., Rehkamper, M., Rouxel, O., Sohrin, Y., Stirling, C., Thompson, C., Vance, D., Xue, Z., and Zhao, Y.: GEOTRACES IC1 (BATS) contamination-prone trace element isotopes Cd, Fe, Pb, Zn, Cu, and Mo intercalibration, Limnol. Oceanogr.-Meth., 10, 653–665, https://doi.org/10.4319/lom.2012.10.653, 2012.

Bruch, W., Piazzola, J., Branger, H., van Eijk, A. M. J., Luneau, C., Bourras, D., and Tedeschi, G.: Sea-Spray-Generation Dependence on Wind and Wave Combinations: A Laboratory Study, Bound.-Lay. Meteorol., 180, 477–505, https://doi.org/10.1007/s10546-021-00636-y, 2021.

Brunskill, G. J.: New Guinea and its coastal seas, a testable model of wet tropical coastal processes: an introduction

to Project TROPICS, Cont. Shelf Res., 24, 2273–2295, https://doi.org/10.1016/j.csr.2004.08.001, 2004.

Buck, C. S., Landing, W. M., and Resing, J.: Pacific Ocean aerosols: Deposition and solubility of iron, aluminum, and other trace elements, Mar. Chem., 157, 117–130, https://doi.org/10.1016/j.marchem.2013.09.005, 2013.

Buck, C. S., Aguilar-Islas, A., Marsay, C., Kadko, D., and Landing, W. M.: Trace element concentrations, elemental ratios, and enrichment factors observed in aerosol samples collected during the US GEOTRACES eastern Pacific Ocean transect (GP16), Chem. Geol., 511, 212–224, https://doi.org/10.1016/j.chemgeo.2019.01.002, 2019.

Canil, D. and Lacourse, T.: An estimate for the bulk composition of juvenile upper continental crust derived from glacial till in the North American Cordillera, Chem. Geol., 284, 229–239, https://doi.org/10.1016/j.chemgeo.2011.02.024, 2011.

Chapman, J. B., Weiss, D. J., Shan, Y., and Lemburger, M.: Iron isotope fractionation during leaching of granite and basalt by hydrochloric and oxalic acids, Geochim. Cosmochim. Ac., 73, 1312–1324, https://doi.org/10.1016/j.gca.2008.11.037, 2009.

Chen, T., Li, W., Guo, B., Liu, R., Li, G., Zhao, L., and Ji, J.: Reactive iron isotope signatures of the East Asian dust particles: Implications for iron cycling in the deep North Pacific, Chem. Geol., 531, 119342, https://doi.org/10.1016/j.chemgeo.2019.119342, 2020.

Conway, T. M. and John, S. G.: Quantification of dissolved iron sources to the North Atlantic Ocean, Nature, 511, 212–215, https://doi.org/10.1038/nature13482, 2014.

Conway, T. M., Wolff, E. W., Röthlisberger, R., Mulvaney, R., and Elderfield, H. E.: Constraints on soluble aerosol iron flux to the Southern Ocean at the Last Glacial Maximum, Nat. Commun., 6, 7850, https://doi.org/10.1038/ncomms8850, 2015.

Conway, T. M., John, S. G., and Lacan, F.: Intercomparison of dissolved iron isotope profiles from reoccupation of three GEOTRACES stations in the Atlantic Ocean, Mar. Chem., 183, 50–61, https://doi.org/10.1016/j.marchem.2016.04.007, 2016.

Conway, T. M., Hamilton, D. S., Shelley, R. U., Aguilar-Islas, A. M., Landing, W. M., Mahowald, N. M., and John, S. G.: Tracing and constraining anthropogenic aerosol iron fluxes to the North Atlantic Ocean using iron isotopes, Nat. Commun., 10, 2628, https://doi.org/10.1038/s41467-019-10457-w, 2019.

Craddock, P. R., Warren, J. M., and Dauphas, N.: Abyssal peridotites reveal the near-chondritic Fe isotopic composition of the Earth, Earth Planet. Sc. Lett., 365, 63–76, https://doi.org/10.1016/j.epsl.2013.01.011, 2013.

Dammshäuser, A.: Distribution and behavior of the lithogenic tracers aluminium and titanium in the upper water column of the Atlantic Ocean, Faculty of Mathematics and Natural Sciences Christian-Albrechts-Universität zu Kiel, https://nbn-resolving.org/urn:nbn:de:gbv:8-diss-81211 (last access: 16 November 2024), 2012.

Desboeufs, K.: Processus de dissolution des aérosols atmosphériques au sein des gouttes d'eau nuageuses, Université Paris-Diderot – Paris VII, https://theses.hal.science/tel-00005175 (last access: 18 November 2024), 2001.

Desboeufs, K., Formenti, P., Torres-Sánchez, R., Schepanski, K., Chaboureau, J.-P., Andersen, H., Cermak, J., Feuerstein, S., Laurent, B., Klopper, D., Namwoonde, A., Cazaunau, M., Chevaillier, S., Feron, A., Mirande-Bret, C., Triquet, S., and Piketh, S. J.: Fractional solubility of iron in mineral dust aerosols over coastal Namibia: a link to marine biogenic emissions?, Atmos. Chem. Phys., 24, 1525–1541, https://doi.org/10.5194/acp-24-1525-2024, 2024.

Duce, R. A. and Hoffman, G. L.: Atmospheric vanadium transport to the ocean, Atmos. Environ., 10, 989–996, https://doi.org/10.1016/0004-6981(76)90207-9, 1976.

Duce, R. A. and Tindale, N. W.: Atmospheric transport of iron and its deposition in the ocean, Limnol. Oceanogr., 36, 1715–1726, https://doi.org/10.4319/lo.1991.36.8.1715, 1991.

Elrod, V. A., Berelson, W. M., Coale, K. H., and Johnson, K. S.: The flux of iron from continental shelf sediments: A missing source for global budgets, Geophys. Res. Lett., 31, L12307, https://doi.org/10.1029/2004GL020216, 2004.

Ellwood, M. J., Hutchins, D. A., Lohan, M. C., Milne, A., Nasemann, P., Nodder, S. D., Sander, S. G., Strzepek, R., Wilhelm, S. W., and Boyd, P. W.: Iron stable isotopes track pelagic iron cycling during a subtropical phytoplankton bloom, P. Natl. Acad. Sci. USA, 112, E15–E20, https://doi.org/10.1073/pnas.1421576112, 2015.

Flament, P., Mattielli, N., Aimoz, L., Choël, M., Deboudt, K., Jong, J. de, Rimetz-Planchon, J., and Weis, D.: Iron isotopic fractionation in industrial emissions and urban aerosols, Chemosphere, 73, 1793–1798, https://doi.org/10.1016/j.chemosphere.2008.08.042, 2008.

Hamilton, D. S., Scanza, R. A., Feng, Y., Guinness, J., Kok, J. F., Li, L., Liu, X., Rathod, S. D., Wan, J. S., Wu, M., and Mahowald, N. M.: Improved methodologies for Earth system modelling of atmospheric soluble iron and observation comparisons using the Mechanism of Intermediate complexity for Modelling Iron (MIMI v1.0), Geosci. Model Dev., 12, 3835–3862, https://doi.org/10.5194/gmd-12-3835-2019, 2019.

Hao, Y., Guo, Z., Yang, Z., Fang, M., and Feng, J.: Seasonal variations and sources of various elements in the atmospheric aerosols in Qingdao, China, Atmos. Res., 85, 27–37, https://doi.org/10.1016/j.atmosres.2006.11.001, 2007.

Homoky, W. B., Conway, T. M., John, S. G., König, D., Deng, F., Tagliabue, A., and Mills, R. A.: Iron colloids dominate sedimentary supply to the ocean interior, P. Natl. Acad. Sci. USA, 118, e2016078118, https://doi.org/10.1073/pnas.2016078118, 2021.

Hu, Z. and Gao, S.: Upper crustal abundances of trace elements: A revision and update, Chem. Geol., 253, 205–221, https://doi.org/10.1016/j.chemgeo.2008.05.010, 2008.

Jickells, T., An, Z., Andersen, K., Baker, A., Bergametti, G., Brooks, N., Cao, J., Boyd, P., Duce, R., Hunter, K., Kawahata, H., Kubilay, N., Laroche, J., Liss, P., Mahowald, N., Prospero, J., Ridgwell, A., Tegen, I., and Torres, R.: Global Iron Connections Between Desert Dust, Ocean Biogeochemistry, and Climate, Science, 308, 67–71, https://doi.org/10.1126/science.1105959, 2005.

John, S. G., Mendez, J., Moffett, J., and Adkins, J.: The flux of iron and iron isotopes from San Pedro Basin sediments, Geochim. Cosmochim. Ac., 93, 14–29, https://doi.org/10.1016/j.gca.2012.06.003, 2012.

Kiczka, M., Wiederhold, J. G., Frommer, J., Kraemer, S. M., Bourdon, B., and Kretzschmar, R.: Iron isotope fractionation during proton- and ligand-promoted dissolution of primary phyllosilicates, Geochim. Cosmochim. Ac., 74, 3112–3128, https://doi.org/10.1016/j.gca.2010.02.018, 2010.

Klar, J. K., Schlosser, C., Milton, J. A., Woodward, E. M. S., Lacan, F., Parkinson, I. J., Achterberg, E. P., and James, R. H.: Sources of dissolved iron to oxygen minimum zone waters on the Senegalese continental margin in the tropical North Atlantic Ocean: Insights from iron isotopes, Geochim. Cosmochim. Ac., 236, 60–78, https://doi.org/10.1016/j.gca.2018.02.031, 2018.

Kommalapati, R. R. and Valsaraj, K. T.: Atmospheric Aerosols and Their Importance, in: Atmospheric Aerosols, vol. 1005, American Chemical Society, 1–10, https://doi.org/10.1021/bk-2009-1005.ch001, 2009.

Kurisu, M. and Takahashi, Y.: Testing Iron Stable Isotope Ratios as a Signature of Biomass Burning, Atmosphere-Basel, 10, 76, https://doi.org/10.3390/atmos10020076, 2019.

Kurisu, M., Sakata, K., Miyamoto, C., Takaku, Y., Iizuka, T., and Takahashi, Y.: Variation of Iron Isotope Ratios in Anthropogenic Materials Emitted through Combustion Processes, Chem. Lett., 45, 970–972, https://doi.org/10.1246/cl.160451, 2016a.

Kurisu, M., Takahashi, Y., Iizuka, T., and Uematsu, M.: Very low isotope ratio of iron in fine aerosols related to its contribution to the surface ocean, J. Geophys. Res.-Atmos., 121, 11119–11136, https://doi.org/10.1002/2016JD024957, 2016b.

Kurisu, M., Sakata, K., Uematsu, M., Ito, A., and Takahashi, Y.: Contribution of combustion Fe in marine aerosols over the northwestern Pacific estimated by Fe stable isotope ratios, Atmos. Chem. Phys., 21, 16027–16050, https://doi.org/10.5194/acp-21-16027-2021, 2021.

Kurisu, M., Sakata, K., Nishioka, J., Obata, H., Conway, T. M., Hunt, H. R., Sieber, M., Suzuki, K., Kashiwabara, T., Kubo, S., Takada, M., and Takahashi, Y.: Source and fate of atmospheric iron supplied to the subarctic North Pacific traced by stable iron isotope ratios, Geochim. Cosmochim. Ac., 378, 168–185, https://doi.org/10.1016/j.gca.2024.06.009, 2024.

Labatut, M., Lacan, F., Pradoux, C., Chmeleff, J., Radic, A., Murray, J. W., Poitrasson, F., Johansen, A. M., and Thil, F.: Iron sources and dissolved-particulate interactions in the seawater of the Western Equatorial Pacific, iron isotope perspectives, Global Biogeochem. Cy., 28, 1044–1065, https://doi.org/10.1002/2014GB004928, 2014.

Lacan, F., Radic, A., Jeandel, C., Poitrasson, F., Sarthou, G., Pradoux, C., and Freydier, R.: Measurement of the isotopic composition of dissolved iron in the open ocean, Geophys. Res. Lett., 35, L24610, https://doi.org/10.1029/2008GL035841, 2008.

Lacan, F., Radic, A., Labatut, M., Jeandel, C., Poitrasson, F., Sarthou, G., Pradoux, C., Chmeleff, J., and Freydier, R.: High-Precision Determination of the Isotopic Composition of Dissolved Iron in Iron Depleted Seawater by Double Spike Multicollector-ICPMS, Anal. Chem., 82, 7103–7111, https://doi.org/10.1021/ac1002504, 2010.

Lacan, F., Artigue, L., Klar, J. K., Pradoux, C., Chmeleff, J., and Freydier, R.: Interferences and Matrix Effects on Iron Isotopic Composition Measurements by ^{57}Fe–^{58}Fe Double-Spike Multi-Collector Inductively Coupled Plasma Mass Spectrometry; the Importance of Calcium and Aluminum Interferences, Front. Environ. Chem., 2, 692025, https://doi.org/10.3389/fenvc.2021.692025, 2021.

Lacan, F., Pradoux, C., Dutrieux, P., Murray, J. W., Johansen, A., Radic, A., and Labatut, M.: CTD, dissolved oxygen concentrations, iron concentrations and isotopic compositions in the filtered seawater, seawater suspended particles and aerosols, during the EUCFe cruise, KM0625, in the Equatorial Pacific Ocean, SEANOE [data set], https://doi.org/10.17882/107774, 2025.

Landing, W. M. and Shelley, R.: Total aerosol trace metal concentrations from R/V *Knorr* cruises KN199-04 and KN204-01 in the Subtropical northern Atlantic Ocean from 2010–2011, U.S. GEOTRACES NAT project [data set], Version 16 September 2014, http://lod.bco-dmo.org/id/dataset/3865 (last access: 30 November 2024), 2014.

Landing, W. M., Measures, C. I., and Resing, J. A.: Collaborative Research: Global Ocean Survey of Dissolved Iron and Aluminum and Aerosol Iron and Aluminum Solubility Supporting the Repeat Hydrography (CO_2 Project (CLIVAR AEROSOL) [data set], Version 12 June 2013, https://www.bco-dmo.org/dataset-deployment/454424 (last access: 30 November 2024), 2013.

Lelieveld, J. and Crutzen, P. J.: The role of clouds in tropospheric photochemistry, J. Atmos. Chem., 12, 229–267, https://doi.org/10.1007/BF00048075, 1991.

Li, R., Zhang, H., Wang, F., He, Y., Huang, C., Luo, L., Dong, S., Jia, X., and Tang, M.: Mass fractions, solubility, speciation and isotopic compositions of iron in coal and municipal waste fly ash, Sci. Total Environ., 838, 155974, https://doi.org/10.1016/j.scitotenv.2022.155974, 2022.

Madawala, C. K., Molina, C., Kim, D., Gamage, D. K., Sun, M., Leibensperger, R. J. I., Mehndiratta, L., Lee, J., Kaluarachchi, C. P., Kimble, K. A., Sandstrom, G., Harb, C., Dinasquet, J., Malfatti, F., Prather, K. A., Deane, G. B., Stokes, M. D., Lee, C., Slade, J. H., Stone, E. A., Grassian, V. H., and Tivanski, A. V.: Effects of Wind Speed on Size-Dependent Morphology and Composition of Sea Spray Aerosols, ACS Earth Space Chem., 8, 1609–1622, https://doi.org/10.1021/acsearthspacechem.4c00119, 2024.

Majestic, B. J., Anbar, A. D., and Herckes, P.: Elemental and iron isotopic composition of aerosols collected in a parking structure, Sci. Total Environ., 407, 5104–5109, https://doi.org/10.1016/j.scitotenv.2009.05.053, 2009.

Marsay, C. M., Kadko, D., Landing, W. M., and Buck, C. S.: Bulk Aerosol Trace Element Concentrations and Deposition Fluxes During the U.S. GEOTRACES GP15 Pacific Meridional Transect, Global Biogeochem. Cy., 36, e2021GB007122, https://doi.org/10.1029/2021GB007122, 2022.

Martin, J. H.: Iron as a Limiting Factor in Oceanic Productivity, in: Primary Productivity and Biogeochemical Cycles in the Sea, edited by: Falkowski, P. G., Woodhead, A. D., and Vivirito, K., Springer, Boston, MA, 123–137, https://doi.org/10.1007/978-1-4899-0762-2_8, 1992.

Maters, E. C., Mulholland, D. S., Flament, P., de Jong, J., Mattielli, N., Deboudt, K., Dhont, G., and Bychkov, E.: Laboratory study of iron isotope fractionation during dissolution of mineral dust and industrial ash in simulated cloud water, Chemosphere, 299, 134472, https://doi.org/10.1016/j.chemosphere.2022.134472, 2022.

Mead, C., Herckes, P., Majestic, B. J., and Anbar, A. D.: Source apportionment of aerosol iron in the marine environment using iron isotope analysis, Geophys. Res. Lett., 40, 5722–5727, https://doi.org/10.1002/2013GL057713, 2013.

Moore, J. K. and Braucher, O.: Sedimentary and mineral dust sources of dissolved iron to the world ocean, Biogeosciences, 5, 631–656, https://doi.org/10.5194/bg-5-631-2008, 2008.

Morel, F. M. M., Lam, P. J., and Saito, M. A.: Trace Metal Substitution in Marine Phytoplankton, Annu. Rev. Earth Pl. Sc., 48, 491–517, https://doi.org/10.1146/annurev-earth-053018-060108, 2020.

Mulholland, D. S., Flament, P., de Jong, J., Mattielli, N., Deboudt, K., Dhont, G., and Bychkov, E.: In-cloud processing as a possible source of isotopically light iron from anthropogenic aerosols: New insights from a laboratory study, Atmos. Environ., 259, 118505, https://doi.org/10.1016/j.atmosenv.2021.118505, 2021.

Neall, V. E. and Trewick, S. A.: The age and origin of the Pacific islands: a geological overview, Philos. T. R. Soc. B, 363, 3293–3308, https://doi.org/10.1098/rstb.2008.0119, 2008.

Nozaki, Y.: A fresh look at element distribution in the North Pacific Ocean, Eos, Transactions American Geophysical Union, 78, 221–221, https://doi.org/10.1029/97EO00148, 1997.

Nusantara, L.: An outline of the geology of Indonesia, Ikatan Ahli Geologi Indonesia, ISBN 979-8126-04-1, 2000.

Poitrasson, F.: On the iron isotope homogeneity level of the continental crust, Chem. Geol., 235, 195–200, https://doi.org/10.1016/j.chemgeo.2006.06.010, 2006.

Poulton, S. W. and Raiswell, R.: The low-temperature geochemical cycle of iron: From continental fluxes to marine sediment deposition, Am. J. Sci., 302, 774–805, https://doi.org/10.2475/ajs.302.9.774, 2002.

Radic, A., Lacan, F., and Murray, J. W.: Iron isotopes in the seawater of the equatorial Pacific Ocean: New constraints for the oceanic iron cycle, Earth Planet. Sc. Lett., 306, 1–10, https://doi.org/10.1016/j.epsl.2011.03.015, 2011.

Raiswell, R., Benning, L. G., Tranter, M., and Tulaczyk, S.: Bioavailable iron in the Southern Ocean: the significance of the iceberg conveyor belt, Geochem. T., 9, 7, https://doi.org/10.1186/1467-4866-9-7, 2008.

Ramos, V. A.: Anatomy and global context of the Andes: Main geologic features and the Andean orogenic cycle, in: Backbone of the Americas: Shallow Subduction, Plateau Uplift, and Ridge and Terrane Collision, edited by: Kay, S. M., Ramos, V. A., and Dickinson, W. R., Geological Society of America, https://doi.org/10.1130/2009.1204(02), 2009.

Resing, J. A., Sedwick, P. N., German, C. R., Jenkins, W. J., Moffett, J. W., Sohst, B. M., and Tagliabue, A.: Basin-scale transport of hydrothermal dissolved metals across the South Pacific Ocean, Nature, 523, 200–203, https://doi.org/10.1038/nature14577, 2015.

Rolph, G., Stein, A., and Stunder, B.: Real-time Environmental Applications and Display sYstem: READY, Environ. Modell. Softw., 95, 210–228, https://doi.org/10.1016/j.envsoft.2017.06.025, 2017.

Rudnick, R. L. and Gao, S.: 4.1 – Composition of the Continental Crust, in: Treatise on Geochemistry, 2nd edn., edited by: Holland, H. D. and Turekian, K. K., Elsevier, Oxford, 51 pp., https://doi.org/10.1016/B978-0-08-095975-7.00301-6, 2014.

Sakata, K., Kurisu, M., Takeichi, Y., Sakaguchi, A., Tanimoto, H., Tamenori, Y., Matsuki, A., and Takahashi, Y.: Iron (Fe) speciation in size-fractionated aerosol particles in the Pacific Ocean: The role of organic complexation of Fe with humic-like substances in controlling Fe solubility, Atmos. Chem. Phys., 22, 9461–9482, https://doi.org/10.5194/acp-22-9461-2022, 2022.

Seinfeld, J. H. and Pandis, S. N.: Atmospheric Chemistry and Physics: From Air Pollution to Climate Change, John Wiley and Sons, ISBN 978-1-118-94740-1, 2006.

Shah, V., Jacob, D. J., Moch, J. M., Wang, X., and Zhai, S.: Global modeling of cloud water acidity, precipitation acidity, and acid inputs to ecosystems, Atmos. Chem. Phys., 20, 12223–12245, https://doi.org/10.5194/acp-20-12223-2020, 2020.

Shelley, R. U., Roca-Martí, M., Castrillejo, M., Sanial, V., Masqué, P., Landing, W. M., van Beek, P., Planquette, H., and Sarthou, G.: Quantification of trace element atmospheric deposition fluxes to the Atlantic Ocean (> 40° N; GEOVIDE, GEOTRACES GA01) during spring 2014, Deep-Sea Res. Pt. I, 119, 34–49, https://doi.org/10.1016/j.dsr.2016.11.010, 2017.

Shelley, R. U., Landing, W. M., Ussher, S. J., Planquette, H., and Sarthou, G.: Regional trends in the fractional solubility of Fe and other metals from North Atlantic aerosols (GEOTRACES cruises GA01 and GA03) following a two-stage leach, Biogeosciences, 15, 2271–2288, https://doi.org/10.5194/bg-15-2271-2018, 2018.

Sholkovitz, E. R., Sedwick, P. N., Church, T. M., Baker, A. R., and Powell, C. F.: Fractional solubility of aerosol iron: Synthesis of a global-scale data set, Geochim. Cosmochim. Ac., 89, 173–189, https://doi.org/10.1016/j.gca.2012.04.022, 2012.

Slemons, L., Gorgues, T., Aumont, O., Menkes, C., and Murray, J. W.: Biogeochemical impact of a model western iron source in the Pacific Equatorial Undercurrent, Deep-Sea Res. Pt. I, 56, 2115–2128, https://doi.org/10.1016/j.dsr.2009.08.005, 2009.

Slemons, L., Murray, J. W., Resing, J., Paul, B., and Dutrieux, P.: Western Pacific coastal sources of iron, manganese, and aluminum to the Equatorial Undercurrent, Global Biogeochem. Cy., 24, GB3024, https://doi.org/10.1029/2009GB003693, 2010.

Slemons, L., Paul, B., Resing, J., and Murray, J. W.: Particulate iron, aluminum, and manganese in the Pacific equatorial undercurrent and low latitude western boundary current sources, Mar. Chem., 142–144, 54–67, https://doi.org/10.1016/j.marchem.2012.08.003, 2012.

Stein, A. F., Draxler, R. R., Rolph, G. D., Stunder, B. J. B., Cohen, M. D., and Ngan, F.: NOAA's HYSPLIT Atmospheric Transport and Dispersion Modeling System, B. Am. Meteorol. Soc., 96, 2059–2077, https://doi.org/10.1175/BAMS-D-14-00110.1, 2015.

Tagliabue, A., Bopp, L., Dutay, J.-C., Bowie, A. R., Chever, F., Jean-Baptiste, P., Bucciarelli, E., Lannuzel, D., Remenyi, T., Sarthou, G., Aumont, O., Gehlen, M., and Jeandel, C.: Hydrothermal contribution to the oceanic dissolved iron inventory, Nat. Geosci., 3, 252–256, https://doi.org/10.1038/ngeo818, 2010.

Teng, F.-Z., Dauphas, N., Huang, S., and Marty, B.: Iron isotopic systematics of oceanic basalts, Geochim. Cosmochim. Ac., 107, 12–26, https://doi.org/10.1016/j.gca.2012.12.027, 2013.

Turekian, K. K. and Wedepohl, K. H.: Distribution of the Elements in Some Major Units of the Earth's Crust, GSA Bulletin, 72, 175–192, https://doi.org/10.1130/0016-7606(1961)72[175:DOTEIS]2.0.CO;2, 1961.

Waeles, M., Baker, A. R., Jickells, T., and Hoogewerff, J.: Global dust teleconnections: aerosol iron solubility and stable isotope composition, Environ. Chem., 4, 233, https://doi.org/10.1071/EN07013, 2007.

Wang, Y., Wu, L., Hu, W., Li, W., Shi, Z., Harrison, R. M., and Fu, P.: Stable iron isotopic composition of atmospheric aerosols: An overview, NPJ

Wei, T., Dong, Z., Zong, C., Liu, X., Kang, S., Yan, Y., and Ren, J.: Global-scale constraints on the origins of aerosol iron using stable iron isotopes: A review, Earth-Sci. Rev., 258, 104943, https://doi.org/10.1016/j.earscirev.2024.104943, 2024.

Whitby, K. T.: The physical characteristics of sulfur aerosols, Atmos. Environ., 12, 135–159, https://doi.org/10.1016/0004-6981(78)90196-8, 1978.

Wiederhold, J. G., Kraemer, S. M., Teutsch, N., Borer, P. M., Halliday, A. N., and Kretzschmar, R.: Iron Isotope Fractionation during Proton-Promoted, Ligand-Controlled, and Reductive Dissolution of Goethite, Environ. Sci. Technol., 40, 3787–3793, https://doi.org/10.1021/es052228y, 2006.

Wunderman, R.: Report on Rabaul (Papua New Guinea), Bulletin of the Global Volcanism Network, 31, 9, https://doi.org/10.5479/si.GVP.BGVN200609-252140, 2006.

Yeghicheyan, D., Bossy, C., Bouhnik Le Coz, M., Douchet, C., Granier, G., Heimburger, A., Lacan, F., Lanzanova, A., Rousseau, T. C. C., Seidel, J.-L., Tharaud, M., Candaudap, F., Chmeleff, J., Cloquet, C., Delpoux, S., Labatut, M., Losno, R., Pradoux, C., Sivry, Y., and Sonke, J. E.: A Compilation of Silicon, Rare Earth Element and Twenty-One other Trace Element Concentrations in the Natural River Water Reference Material SLRS-5 (NRC-CNRC), Geostand. Geoanal. Res., 37, 449–467, https://doi.org/10.1111/j.1751-908X.2013.00232.x, 2013.

Yeghicheyan, D., Aubert, D., Bouhnik-Le Coz, M., Chmeleff, J., Delpoux, S., Djouraev, I., Granier, G., Lacan, F., Piro, J.-L., Rousseau, T., Cloquet, C., Marquet, A., Menniti, C., Pradoux, C., Freydier, R., Vieira da Silva-Filho, E., and Suchorski, K.: A New Interlaboratory Characterisation of Silicon, Rare Earth Elements and Twenty-Two Other Trace Element Concentrations in the Natural River Water Certified Reference Material SLRS-6 (NRC-CNRC), Geostand. Geoanal. Res., 43, 475–496, https://doi.org/10.1111/ggr.12268, 2019.

Zhai, J., Burke, I. T., Mayes, W. M., and Stewart, D. I.: New insights into biomass combustion ash categorisation: A phylogenetic analysis, Fuel, 287, 119469, https://doi.org/10.1016/j.fuel.2020.119469, 2021.

Zoller, W. H., Gladney, E. S., and Duce, R. A.: Atmospheric Concentrations and Sources of Trace Metals at the South Pole, Science, 183, 198–200, https://doi.org/10.1126/science.183.4121.198, 1974.